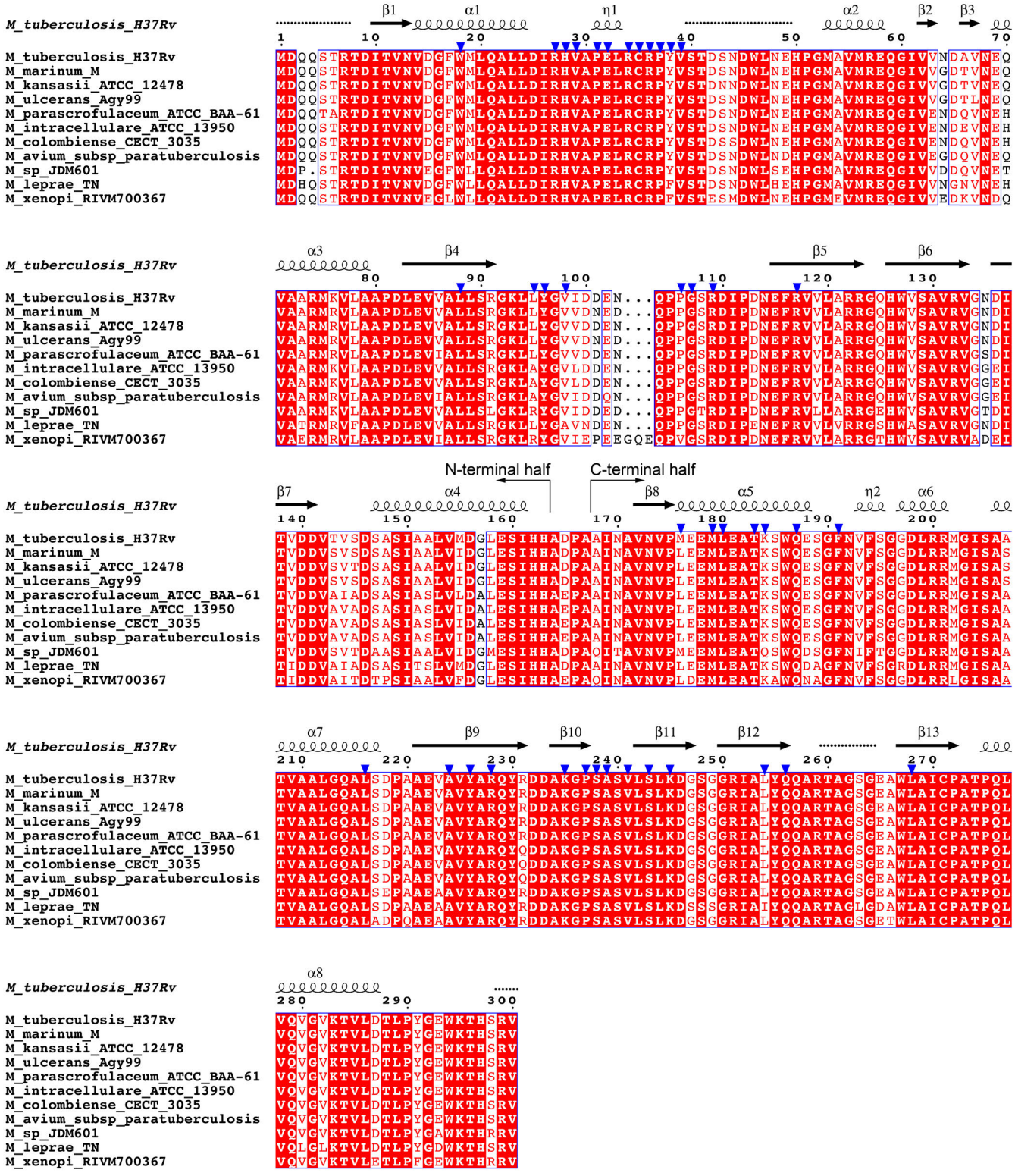

Figure S1. Sequence alignment of the EspG$_5$ family members. Sequences with >98 % identity were excluded from the alignment. Identical residues are highlighted in red. Blue triangles at the top of the alignments indicate residues that are in contact with PPE41 in the *M. tuberculosis* PE25–PPE41–EspG$_5$ complex. The secondary structure elements of *M. tuberculosis* EspG$_5$ are shown at the top of the alignment. Black dashed lines indicate disordered residues.

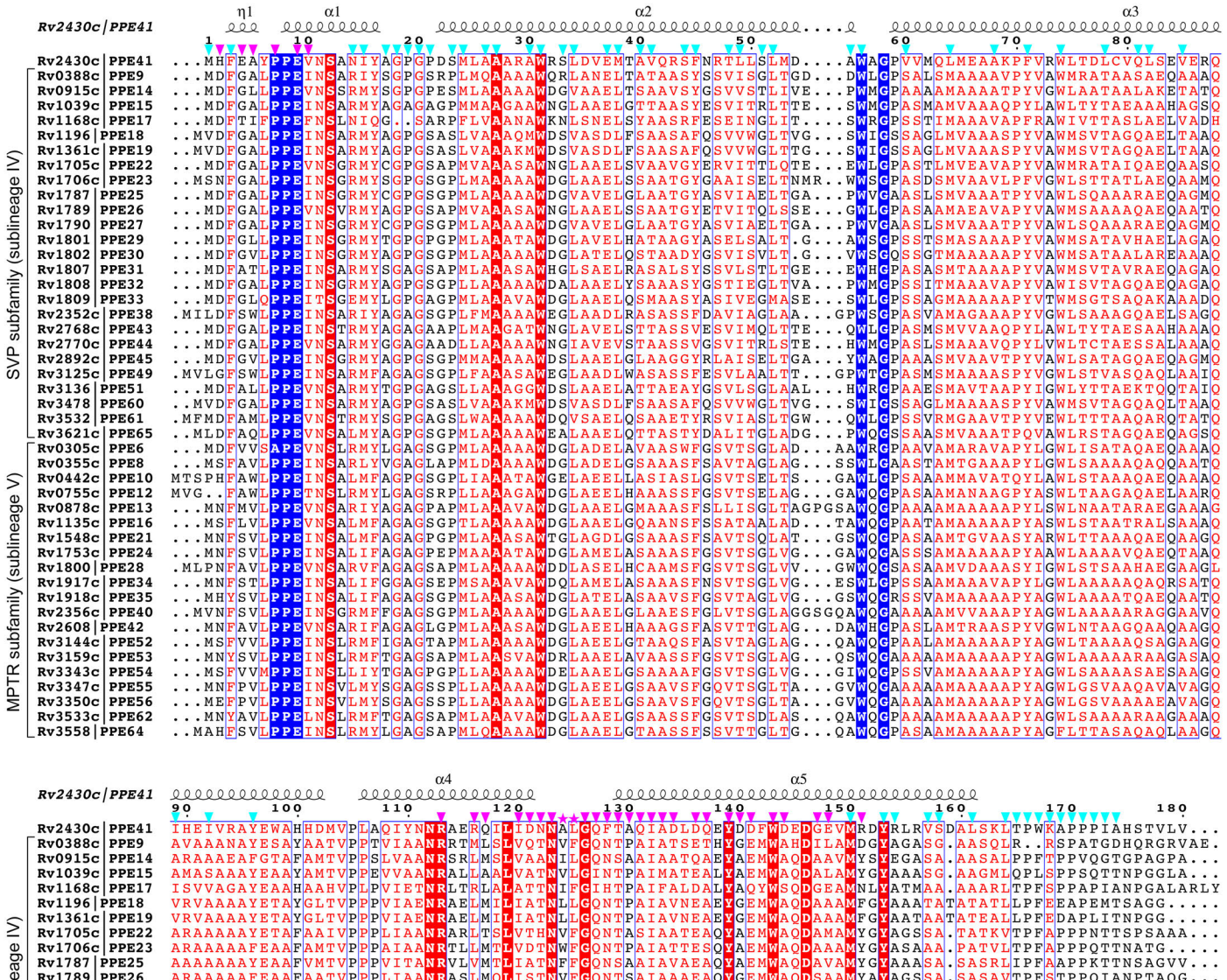

Figure S2. Sequence alignment of the ESX-5-specific PPE proteins from *M. tuberculosis* H37Rv. Only the core PPE domain sequences (~180 residues) are aligned. Identical residues are highlighted in red. The PPE and WxG motifs are highlighted in blue. Residues that are in contact with $EspG_5$ and PE25 in the *M. tuberculosis* PE25–PPE41–$EspG_5$ complex are labeled by purple and cyan triangles, respectively. Purple stars indicate two hydrophobic residues in the α4–α5 loop of PPE proteins that comprise the hh motif. The secondary structure elements of PPE41 are shown at the top of the alignment.

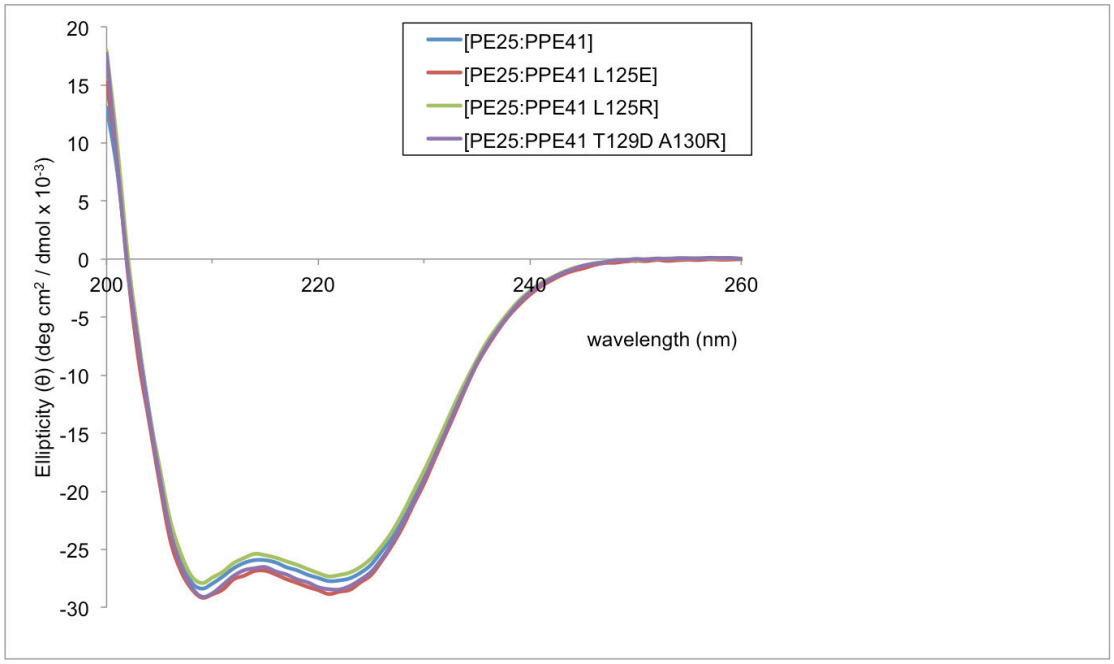

Figure S3. Circular dichroism analysis of the wild-type and mutant PE25–PPE41 complexes. Spectra between wavelengths 200 nm and 260 nm are plotted against mean residue ellipticity. The mutant complexes exhibit a similar secondary structure content as the wild-type PE25–PPE41.

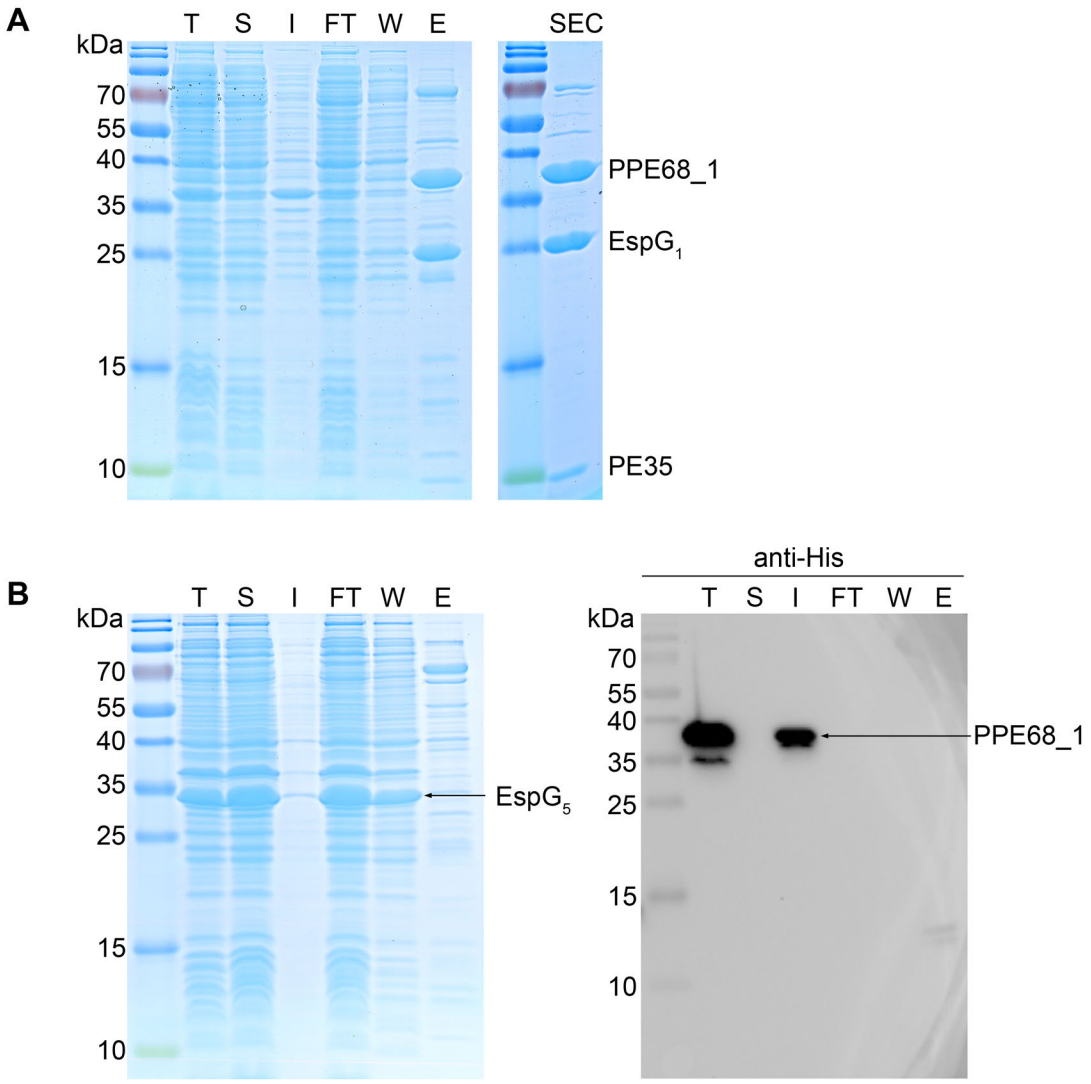

Figure S4. The ESX-1-specific PE35–PPE68_1 dimer interacts with $EspG_1$ but not with $EspG_5$. (A) *M. marinum* PE35, PPE_68-His and $EspG_1$ were co-expressed in *E. coli* and purified using immobilized Ni^{2+} affinity and size-exclusion chromatography. Total cell lysate (T), soluble fraction (S), insoluble fraction (I), flow-through fraction (FT), wash fraction (W), eluted proteins (E) and peak fraction from size-exclusion chromatography (SEC) were analyzed by SDS-PAGE. (B) *M. marinum* PE35, PPE_68-His and $EspG_5$ were co-expressed in *E. coli* and purified using immobilized Ni^{2+} affinity chromatography. Fractions were analyzed by SDS-PAGE and immunoblotting with anti-His tag antibodies. PPE_68-His was found in the insoluble fraction.

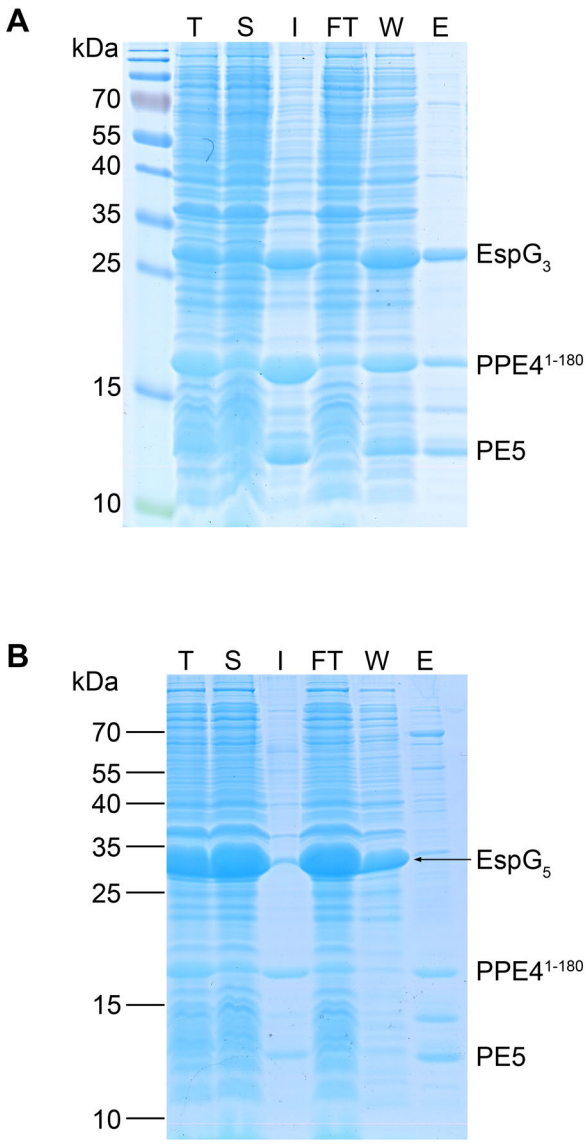

Figure S5. The ESX-3-specific PE5–PPE4 dimer interacts with $EspG_3$ but not with $EspG_5$. (A) *M. smegmatis* PE5-His, the core domain of PPE4 (residues 1–180) and $EspG_3$ were co-expressed in *E. coli* and purified using immobilized Ni^{2+} affinity chromatography. Total cell lysate (T), soluble fraction (S), insoluble fraction (I), flow-through fraction (FT), wash fraction (W) and eluted proteins (E) were analyzed by SDS-PAGE. (B) *M. smegmatis* PE5-His, $PPE4^{1–180}$ and *M. marinum* $EspG_5$ were co-expressed in *E. coli* and purified using immobilized Ni^{2+} affinity chromatography. While PE5–$PPE4^{1–180}$ dimer could be purified, it is unstable and precipitates in the absence of cognate $EspG_3$ chaperone.

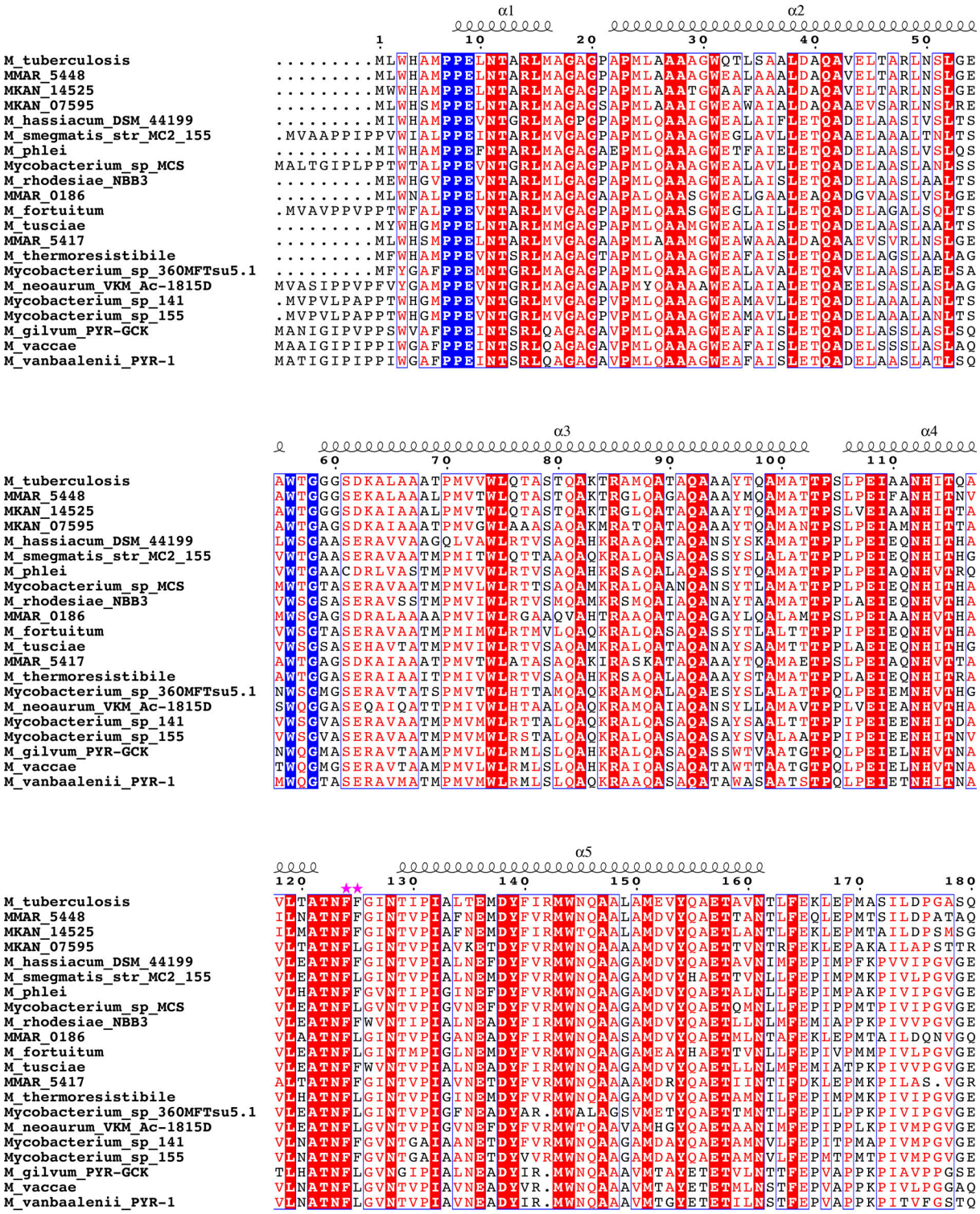

Figure S6. Sequence alignment of PPE68 homologs from *Mycobacteria*. Only the core PPE domain sequences (~180 residues) are aligned. The PPE and WxG motifs are highlighted in blue. The predicted secondary structure elements are shown at the top of the alignments. Purple stars indicate the hh motif. The majority of mycobacterial genomes contain a single PPE68 homolog, whereas *M. marinum* and *M. kansasii* have several PPE68 homologs.

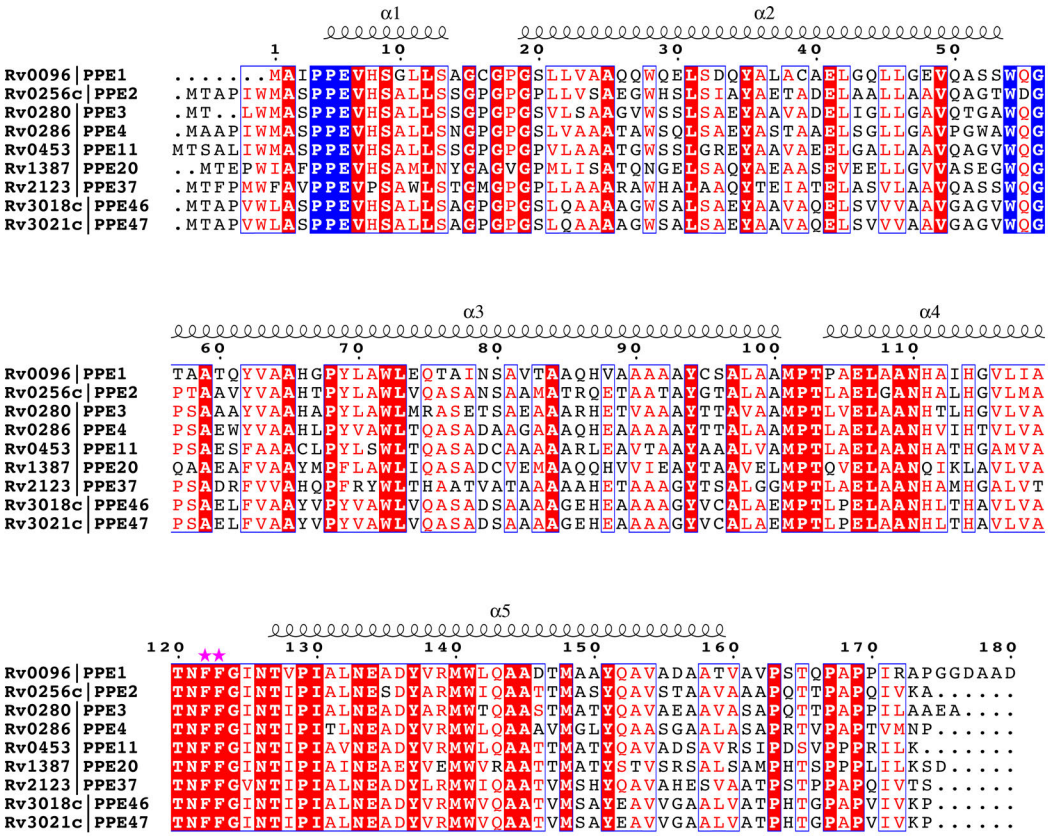

Figure S7. Sequence alignment of the ESX-3-specific PPE proteins from *M. tuberculosis* H37Rv. Only the core PPE domain sequences (~180 residues) are aligned. The PPE and WxG motifs are highlighted in blue. The predicted secondary structure elements are shown at the top. The hh motif is indicated by purple stars.

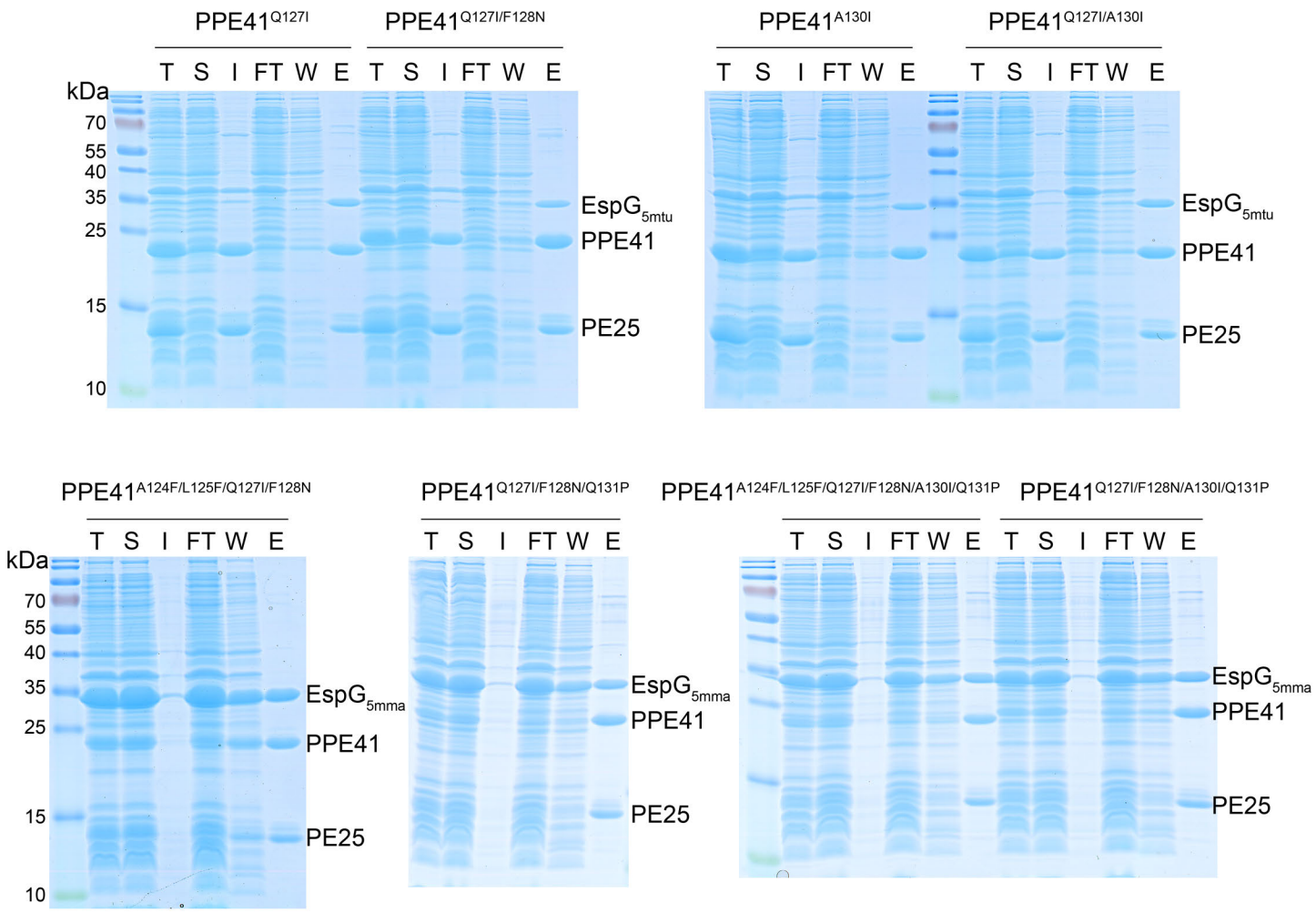

Figure S8. Co-purification of $EspG_5$ and PE25–PPE41 mutant variant dimers. PE25–PPE41 dimers were co-expressed in *E. coli* with either *M. tuberculosis* $EspG_5$ ($EspG_{5mtu}$) or *M. marinum* $EspG_5$ ($EspG_{5mma}$). Proteins were purified using immobilized Ni^{2+} affinity chromatography. Notably, the excess of $EspG_{5mma}$ chaperone leads to complete solubility of PE25–PPE41 with no dimer present in the insoluble fraction.

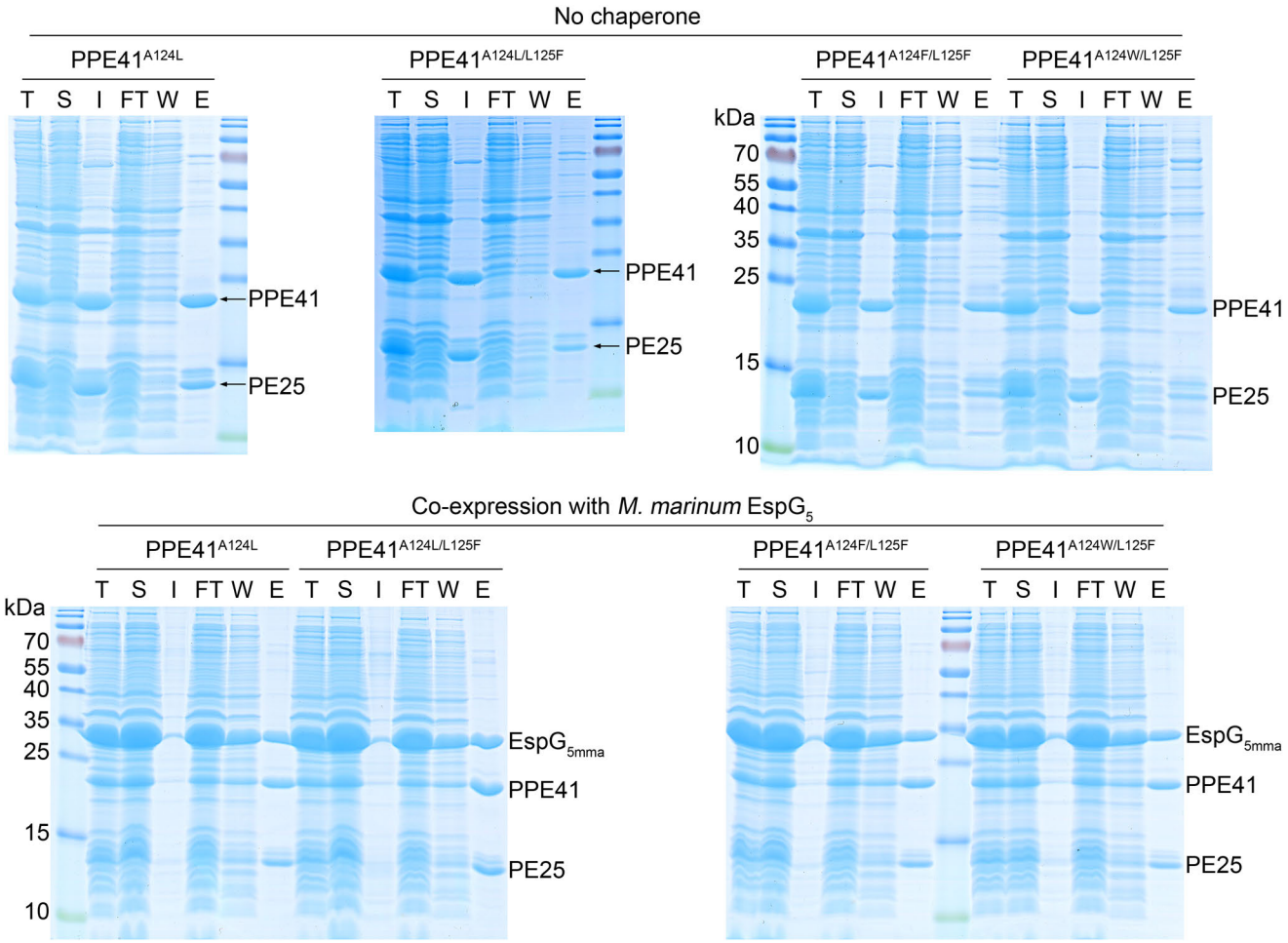

Figure S9. Effect of increased hydrophobicity in the hh motif of PPE41 on protein solubility. PE25–PPE41 dimers were expressed in *E. coli* in the absence of chaperone or co-expressed with *M. marinum* $EspG_5$ ($EspG_{5mma}$). Proteins were purified using immobilized Ni^{2+} affinity chromatography. Total cell lysate (T), soluble fraction (S), insoluble fraction (I), flow-through fraction (FT), wash fraction (W) and eluted proteins (E) were analyzed by SDS-PAGE. Notably, the excess of $EspG_{5mma}$ chaperone leads to complete solubility of PE25–PPE41 with no dimer present in the insoluble fraction.

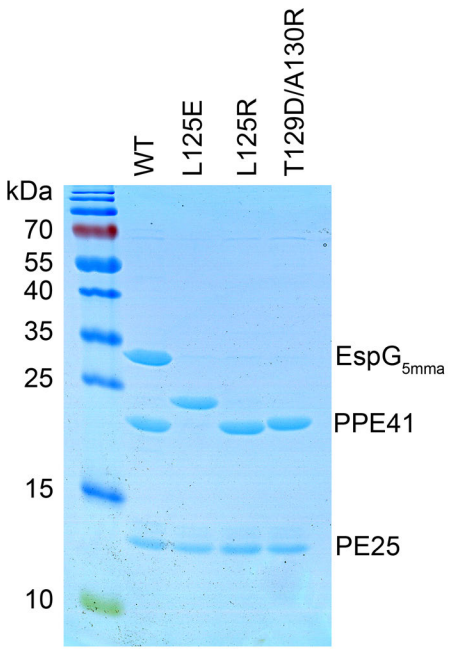

Figure S10. Effect of disruptive mutations in the PPE41 interface on the binding of PE25–PPE41 heterodimer to *M. marinum* $EspG_5$. PE25–PPE41 variants were co-expressed with $EspG_{5mma}$ and purified via immobilized Ni^{2+} affinity chromatography. The results are comparable with *M. tuberculosis* $EspG_5$ binding (Figure 3D).

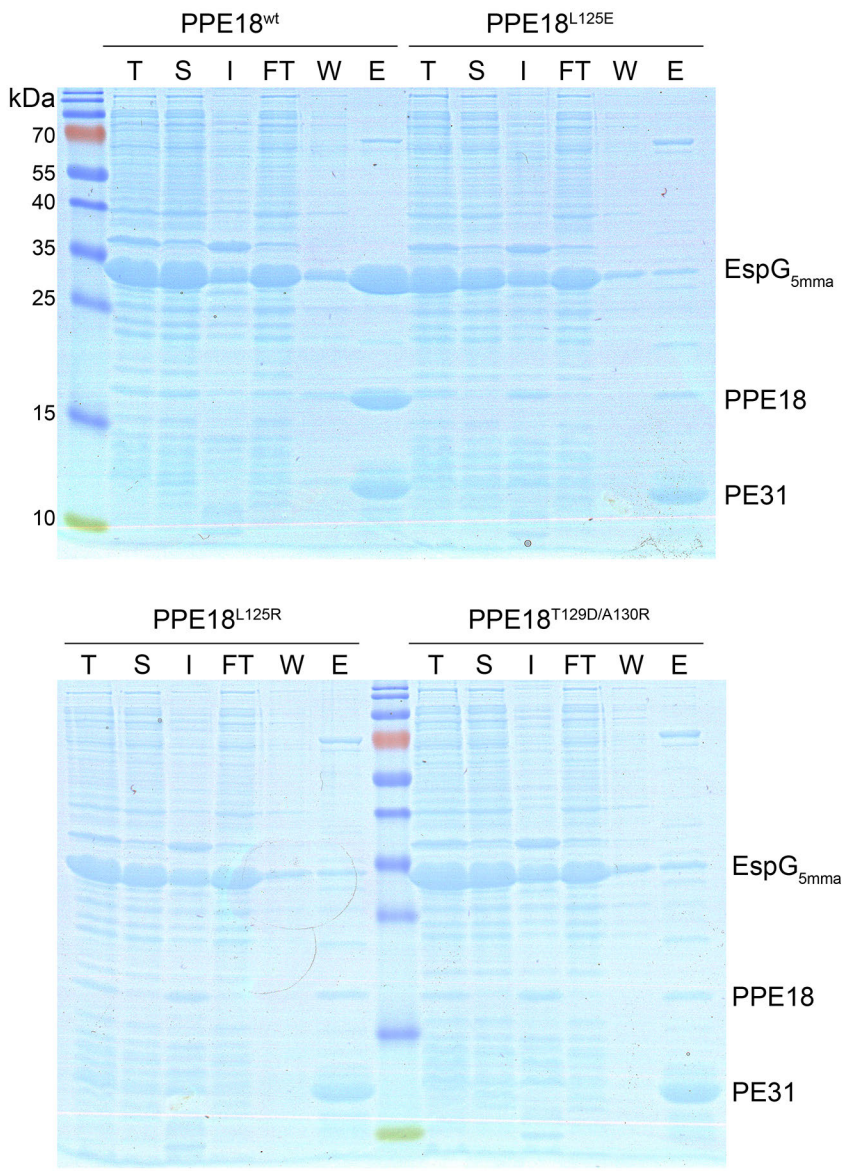

Figure S11. Effect of disruptive mutations in the PPE18 on the binding of PE31–PPE18 heterodimer to *M. marinum* EspG$_5$. PE31–PPE18 variants were co-expressed with EspG$_{5mma}$ and purified via immobilized Ni^{2+} affinity chromatography.

Table S1 Summary of isothermal calorimetry data

Complex	K_d (nM)	ΔH (kcal mol^{-1})	$T\Delta S$ (kcal mol^{-1})	ΔG (kcal mol^{-1})	n
$EspG_5$-PE25-PPE41	48.1±31	-3.4±02	6.8±07	-10.3±0.05	1.08±0.05
$EspG_5$-PE25-PPE41^{L125E}	No binding detectable				
$EspG_5$-PE25-PPE41^{L125R}	No binding detectable				
$EspG_5$-PE25-PPE41$^{T129D/A130R}$	No binding detectable				